11-7-2017

A Budding-Defective M2 Mutant Exhibits Reduced Membrane Interaction, Insensitivity To Cholesterol, And Perturbed Interdomain Coupling

A. L. Herneisen

I. D. Sahu

R. M. McCarrick

See next page for additional authors

Recommended Citation

A. L. Herneisen, I. D. Sahu, R. M. McCarrick, J. B. Feix, G. A. Lorigan, and Kathleen P. Howard. (2017). "A Budding-Defective M2 Mutant Exhibits Reduced Membrane Interaction, Insensitivity To Cholesterol, And Perturbed Interdomain Coupling". *Biochemistry.* Volume 56, Issue 44. 5955-5963. DOI: 10.1021/acs.biochem.7b00924

https://works.swarthmore.edu/fac-chemistry/210

Authors

A. L. Herneisen, I. D. Sahu, R. M. McCarrick, J. B. Feix, G. A. Lorigan, and Kathleen P. Howard

Published in final edited form as:
Biochemistry. 2017 November 07; 56(44): 5955–5963. doi:10.1021/acs.biochem.7b00924.

A Budding-Defective M2 Mutant Exhibits Reduced Membrane Interaction, Insensitivity to Cholesterol, and Perturbed Interdomain Coupling

Alice L. Herneisen[†], **Indra D. Sahu**[‡], **Robert M. McCarrick**[‡], **Jimmy B. Feix**[§], **Gary A. Lorigan**[‡], and **Kathleen P. Howard**[*,†]

[†]Department of Chemistry and Biochemistry, Swarthmore College, Swarthmore, Pennsylvania 19081, United States

[‡]Department of Chemistry and Biochemistry, Miami University, Oxford, Ohio 45056, United States

[§]Department of Biophysics, National Biomedical EPR Center, Medical College of Wisconsin, Milwaukee, Wisconsin 53226, United States

Abstract

Influenza A M2 is a membrane-associated protein with a C-terminal amphipathic helix that plays a cholesterol-dependent role in viral budding. An M2 mutant with alanine substitutions in the C-terminal amphipathic helix is deficient in viral scission. With the goal of providing atomic-level understanding of how the wild-type protein functions, we used a multipronged site-directed spin labeling electron paramagnetic resonance spectroscopy (SDSL-EPR) approach to characterize the conformational properties of the alanine mutant. We spin-labeled sites in the transmembrane (TM) domain and the C-terminal amphipathic helix (AH) of wild-type (WT) and mutant M2, and collected information on line shapes, relaxation rates, membrane topology, and distances within the homotetramer in membranes with and without cholesterol. Our results identify marked differences in the conformation and dynamics between the WT and the alanine mutant. Compared to WT, the dominant population of the mutant AH is more dynamic, shallower in the membrane, and has altered quaternary arrangement of the C-terminal domain. While the AH becomes more dynamic, the dominant population of the TM domain of the mutant is immobilized. The presence of cholesterol changes the conformation and dynamics of the WT protein, while the alanine mutant is insensitive to cholesterol. These findings provide new insight into how M2 may facilitate budding. We propose the AH−membrane interaction modulates the arrangement of the TM helices, effectively stabilizing a conformational state that enables M2 to facilitate viral budding.

---

[*]**Corresponding Author:** E-mail: khoward1@swarthmore.edu.

ASSOCIATED CONTENT
Supporting Information
The Supporting Information is available free of charge on the ACS Publications website at DOI: 10.1021/acs.biochem.7b00924.
Extended Materials and Methods; saturation recovery curves of M2-WT and M2-5Ala site 57; T_1 and j_x values obtained from fits of SR data; PS EPR oxygen accessibility data; hypothetical DEER distance distribution of a homo-tetrameric protein; DEER data of M2-WT and M2-5Ala site 57; comparison of SSNMR model (PDB 2L0J) with experimental DEER data; CD spectra and secondary structure analysis; CW EPR spectra of additional AH sites in + cholesterol membranes; saturation recovery curves of M2-WT and M2-5Ala site 59 in + cholesterol membranes (PDF)

The authors declare no competing financial interest.

Antagonizing the properties of the AH that enable interdomain coupling within M2 may therefore present a novel strategy for anti-influenza drug design.

Abstract

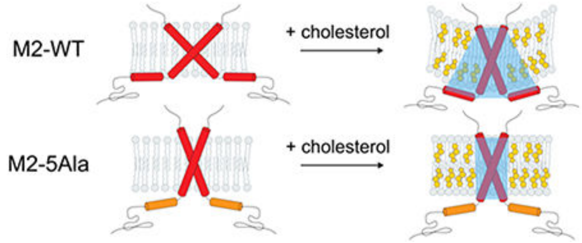

The influenza A virus is a persistent source of morbidity and mortality worldwide.[1,2] An atomic-level understanding of how the virus assembles and buds from the host cell plasma membrane could serve as the basis for new antiviral strategies inhibiting influenza infectivity.[3] Recent studies suggest that the viral coat and core proteins work in concert to promote budding.[3] Here, we examine the conformational properties of one member of the budding machinery, the M2 protein, as well as a mutant deficient in viral budding.

M2 is a homotetrameric, 97-residue membrane-bound protein that orchestrates several essential events in the influenza A infection cycle.[3,4] The determinants for the separate functions of M2 are encoded in different protein domains (Figure 1A). Residues 25−46 associate into a homotetrameric, α-helical transmembrane (TM) domain with ion channel activity necessary for viral uncoating.[4] Less is known about the structure of the N-terminal ectodomain (residues 1−25) and C-terminal cytoplasmic tail (residues 46−97). However, numerous recent studies have explored the role of the C-terminal domain in influenza morphology and infectivity.[5–10]

In particular, recent research efforts have examined the role the M2 cytoplasmic domain plays in viral budding.[12–14] In vitro assays revealed that the full-length M2 protein, as well as just the region spanning residues 46−62, is sufficient to generate the type of curvature necessary for constricting the budding viral neck[15] and induce budding in giant unilamellar vesicles.[12] Several biophysical techniques, including solution NMR,[16,17] solid-state NMR[18,19] (SSNMR), and electron paramagnetic resonance[20,21] (EPR), have demonstrated that M2 residues 47−62 form an amphipathic helix associated with the membrane surface.

Amphipathic helices (AHs) promote membrane remodeling in several systems,[22–24] presumably by inserting into the membrane and reorienting lipids to induce curvature. Several groups have shown that replacing five hydrophobic residues of the M2 AH with alanine—F47A, F48A, I51A, Y52A, and F55A (Figure 1C)—abolishes M2 curvature-generation and budding activity in vitro and leads to a budding-defective morphology in vivo without affecting M2 ion channel function.[12–15,25,26] The penta-alanine mutant, which we designate “M2−5Ala”, offers a valuable opportunity to characterize the structural and dynamic properties of M2 necessary for viral budding.

Several constructs of the M2 protein have been studied by a range of high-resolution biophysical techniques, including X-ray crystallography,[27,28] solution NMR,[16,17] and SSNMR.[18,29–32] The method we employ here, site-directed spin labeling EPR spectroscopy (SDSL-EPR), is a powerful tool for characterizing membrane protein structure and dynamics[33,34] and offers complementary information to previously published structural work on the M2 protein. A strength of SDSL-EPR is the ability to study membrane proteins embedded in lipid bilayers, which is particularly important for characterizing the membrane-remodeling behavior of M2. SDSL-EPR methods can detect mobility and conformational exchange events on time scales not accessible to other spectroscopic techniques,[35] distances in the range of ~12−60 Å,[34] and topology of a protein with respect to the membrane.[33] Our group has used SDSL-EPR to characterize the sensitivity of the M2 TM and AH domains to the surrounding environment.[20,21,36–39] We demonstrated that the M2 AH exists in conformational equilibrium and undergoes cholesterol-dependent conformational exchange.[39] We hy pothesized that this conformational exchange is relevant for M2 scission function at the edge of the viral budozone,[12,13] which is enriched in cholesterol.[40,41]

Here, we seek a structural understanding of the M2-5Ala mutant with the goal of gaining insight into how the wild-type (M2-WT) protein functions. In principle, a detailed understanding of the viral budding process could aid in the development of novel strategies for anti-influenza drug design.

To investigate how the mutations within M2-5Ala impact conformation and dynamics, we spin-labeled sites in both the C-terminal TM and AH domains, and collected SDSL-EPR data. We demonstrate that compared to M2-WT, the dominant population of M2-5Ala is more dynamic, shallower in the membrane, and has an altered quaternary arrangement of the C-terminal domain. Whereas M2-WT experiences notable changes in conformation, dynamics, and membrane topology upon the addition of cholesterol, M2-5Ala remains insensitive to the presence of cholesterol. Our data are consistent with the AHs sensing the properties of the membrane and regulating the arrangement of the TM helices, effectively stabilizing an overall shape of the protein optimal for viral budding.

MATERIALS AND METHODS

Purification, Spin Labeling, and Membrane Reconstitution of Full-Length M2-WT and M2−5Ala Cysteine Mutants.

Cysteine substitutions were introduced into a cysteineless background plasmid based on the A/Udorn/72 sequence,[42] referred to as “M2-WT”, using site-directed mutagenesis. The F47A, F48A, I51A, Y52A, and F55A mutations were introduced into the M2-WT plasmid to generate the “M2-5Ala” plasmid, which was used for further cysteine mutagenesis. Verified single-cysteine plasmids were transformed into C43 competent cells for protein expression. Expression, purification, and spin labeling were performed according to previously published protocols[21] with minor modifications described in the Supporting Information Materials and Methods. The purity of protein was verified using sodium dodecyl sulfate polyacrylamide gel electrophoresis (SDS-PAGE).

We spin-labeled sites in the C-terminal TM and AH domain of M2-WT and M2-5Ala (Figure 1). To probe properties of the TM, we labeled site L43. This residue faces away from the pore of the channel, and previous electrophysiology studies of full-length M2 demonstrated that cysteine mutagenesis at this site does not significantly affect ion channel behavior.[43,44] To probe the properties of the AH, we labeled a site on each face of the helix (H57 and L59).

Protein was reconstituted into 4:1 1-palmitoyl-2-oleoyl-snglycero-3-phosphocholine/-palmitoyl-2-oleoyl-sn-glycero-3-phospho-1-rac-glycerol (POPC/POPG; "− cholesterol") and 56:14:30 POPC/POPG/cholesterol ("+ cholesterol") lipid bilayers as previously described.[21] This membrane system was chosen for its use in in vitro budding assays[12] and previous SDSL-EPR studies of the M2 protein.[20,21,37,39]

EPR Spectroscopy and Data Analysis.

Continuous Wave EPR Spectra.—Continuous wave EPR (CW EPR) spectra were recorded at room temperature on an X-band Bruker EMX spectrometer equipped with an ER4123S resonator. Proteoliposomes were prepared at a peptide/lipid ratio of 1:500 in 50 mM Tris, pH 7.8, 100 mM KCl, 1 mM EDTA buffer. Samples were placed in 0.6 mm internal diameter, 0.9 mm length gas permeable capillary tubes (L&M EPR Supplies, Milwaukee, WI). CW EPR spectra were acquired using 2 mW incident microwave power, 1 G field modulation amplitude at 100 kHz, and 150 G sweep width.

Paramagnetic Accessibility Measurements.—Power saturation experiments were used to detect the oxygen accessibility of spin labels.[45] Experiments were run at room temperature on an X-band Bruker EMX spectrometer equipped with an ER4123S resonator. Proteoliposomes were prepared at a peptide/lipid ratio of 1:500 in 50 mM Tris, pH 7.8, 100 mM KCl, 1 Mm EDTA buffer. Samples were placed in 0.6 mm internal diameter by 0.9 mm length gas permeable capillary tubes (L&M EPR Supplies, Milwaukee, WI). Power saturation experiments were performed under nitrogen gas or equilibrated with ambient air. EPR spectra were collected over eight power levels for nitrogen power saturation experiments. For oxygen power saturation experiments, spectra were collected over 16 or 19 power levels for sites with moderate or high accessibility to oxygen, respectively. Data were fit to obtain $\Delta P_{1/2}$ parameters as described previously.[20]

Saturation Recovery Measurements.—Saturation recovery EPR (SR EPR) experiments were carried out at the National Biomedical EPR Center (Milwaukee, WI) on a home-built instrument operating at X-band (9.4 GHz) equipped with a loop-gap resonator, as previously described.[39] The resulting SR signals were fitted with single- and biexponential decay functions using Origin software (OriginLab, Northampton, MA). Bimolecular collision rates with oxygen, $W_x(O_2)$, were calculated from spin−lattice relaxation rates (W_e) according to the relationship $W_x(O_2) = W_e(O_2) - W_e(N_2)$, where $W_e = 1/2T_1$.

Double Electron−Electron Resonance Measurements.—Double electron−electron resonance (DEER) experiments were carried out at the Ohio Advanced EPR Laboratory at Miami University, Ohio, on a Bruker ELEXSYS E580 spectrometer equipped with a

SuperQ-FT pulse Q-band system with a 10 W amplifier and EN5107D2 resonator. DEER samples were prepared as lipodisq nanoparticles with a peptide/lipid ratio of 1:300, as previously described.[39,46] All DEER samples were prepared at a spin label concentration of 100−130 μM. Glycerol (30% w/w) was used as a cryoprotectant. The sample was loaded into a 1.1 mm inner diameter quartz capillary (Wilmad LabGlass, Buena, NJ) and mounted into the sample holder inserted into the resonator. DEER data were collected using the standard four-pulse sequence[24] $[(\pi/2)_{\nu 1} - \tau_1 - (\pi)_{\nu 1} - t - (\pi)_{\nu 2} - (\tau_1 + \tau_2 - t) - (\pi)_{\nu 1} - \tau_2 - \text{echo}]$ at Q-band with a probe pulse width of 10/20 ns, pump pulse width of 24 ns, 80 MHz of frequency difference between probe and pump pulse, shot repetition time determined by spin−lattice relaxation rate (T_1), 100 echoes/point, and 2-step phase cycling at 80 K collected out to ~2.0 μs for overnight data acquisition time (~12 h). DEER data were analyzed using DEER Analysis 2015.[47] The distance distributions, P(r), were obtained by Tikhonov regularization[48] in the distance domain, incorporating the constraint $P(r) > 0$. A homogeneous two-dimensional model was used for background correction. The regularization parameter in the L curve was optimized by examining the fit of the time domain.

Circular Dichroism Spectroscopy and Data Analysis.

CD spectra were collected on an Aviv model 435 circular dichroism spectrometer at 25 °C. Samples had a protein/lipid ratio of 1:200 and were reconstituted into bicelles.[17] Bicelles with a q = 0.5 were prepared through the addition of 1,2-dihexanoyl-sn-glycero-3-phosphocholine (DHPC) to protein reconstituted in POPC/POPG 4:1 liposomes. The buffer used to collect CD data was 10 mM Tris, pH 7.8, 20 mM KCl, 1 mM EDTA. A 35 μL aliquot of sample was loaded into 0.011 cm path length demountable quartz cuvette. Spectra were collected from 280 to 190 nm with a 1.0 nm step size. The averaging time at each point was 10.0 s, and the bandwidth was 1.0 nm. Three scans were collected and averaged. A bicelle spectrum collected in the absence of protein was used to correct for background due to lipids and buffer. Spectral data collected directly from the instrument were converted from units of millidegrees to per residue molar absorption units ($\Delta\varepsilon$, in units of M^{-1} cm^{-1}). Secondary structure estimates were obtained from the DichroWeb server[49] using the CDSSTR analysis program[50] and a reference set appropriate for membrane proteins.[51,52]

RESULTS

Alanine Mutations Lead to Large Changes in Mobility.

TM is Immobilized in M2−5Ala Relative to M2-WT.—To probe the impact of the C-terminal alanine mutations on the TM domain, we spin-labeled a site located at the end of the TM helix just prior to the start of the AH (L43; Figure 1). The spectral line shapes of spin-labeled residues provide insight into conformational dynamics that reflect both backbone motion as well as secondary and tertiary contacts.[45]

In Figure 2 (top), we show an overlay of the CW EPR spectra of the TM site 43 in both M2-WT (black) and M2− 5Ala (red). The spectra are a superposition of a broad, immobilized component (i), and a sharper, mobile component (m). In a previous study of M2, we characterized the multicomponent nature of M2-WT CW line shapes and established that they arose from an equilibrium involving two different conformational substates of the protein.[39] The M2-5Ala spectrum shown in Figure 2 exhibits a more prominent immobile (i) peak than the corresponding M2-WT site, indicating that the equilibrium of the mutant TM helices is shifted markedly toward an immobile population.

AH Is More Dynamic in M2-5Ala Relative to M2-WT.—To probe the properties of the AH region of M2-5Ala, we spin-labeled a site on each face of the AH (H57 and L59; Figure 1). In Figure 2, we show an overlay of the CW EPR spectra of M2-WT and M2-5Ala for AH sites 57 and 59. For both these AH sites, the mobile spectral component (m) is considerably more pronounced in M2-5Ala. Thus, the equilibria of the TM and AH in M2-5Ala shift in opposite directions relative to M2-WT: while the immobile component is more populated in the M2-5Ala TM, in the M2-5Ala AH, the immobile component is less populated.

Both M2-5Ala and M2-WT are in Conformational Equilibrium.

In a previous study of M2, we used SR EPR to demonstrate that multicomponent CW line shapes, similar to those shown in Figure 2, arose from an equilibrium involving two different conformational substates of the M2 protein.[39] In our earlier work, we used a truncated construct, M2-WT(23−60). To confirm that conformational exchange is indeed a property of the full-length protein, and not an artifact of using a truncation, we collected SR data for both full-length M2-WT as well as M2-5Ala.

In an SR experiment, an intense saturating pulse is applied at the frequency of the central resonance line of the nitroxide. In a spin label system undergoing fast rotameric exchange, the signal recovery is monoexponential. In contrast, spin labels in conformational exchange undergo a biexponential recovery.[35,39]

As shown in Figure 3, the SR curves for both M2-WT (Figure 3A) and M2-5Ala (Figure 3B) are best characterized by a biexponential recovery. Furthermore, the T_1 values obtained from the fits are consistent with protein conformational exchange (Table S1).[35] Biexponential recovery consistent with protein conformational exchange was also obtained for site 57 in both M2-WT and M2-5Ala (Figure S1; Table S1).

The Dominant Population of the M2-5Ala AH Is further from the Membrane Surface.

It has been hypothesized that the loss of budding function for M2-5Ala results from decreased interaction of the AH with the membrane surface due to the reduction in the hydrophobic moment of the AH helix (Figure 1B,C).[12,13] To test this hypothesis, we probed the membrane depth of the M2-5Ala AH using two complementary EPR methods, SR and power saturation.

The spin−lattice relaxation rates measured using SR techniques can be modulated by the presence of paramagnetic relaxation agents such as oxygen. The relaxation rate of the nitroxide spin label, W_e, is proportional to the collision rate of the label with the relaxation agent.[35] Oxygen is a lipophilic species that partitions in a gradient across the membrane, with the highest O_2 concentration at the center of the bilayer. An accessibility constant, j_x, that reports on the membrane accessibility of the spin label can be obtained by measuring W_x at several different O_2 concentrations and calculating the slope of a linear best-fit line.[35]

The insets of Figures 3 and S1 show the dependence of the spin−lattice relaxation rates on the concentration of oxygen for M2-WT and M2-5Ala. The j_x value of the M2-5Ala fast component is notably smaller than that of M2-WT (Figure 3C; Table S1), indicating that the M2-5Ala mobile conformation has AHs shallower in the membrane than the corresponding M2-WT conformation. The j_x values of the M2-WT and M2−5Ala slow components are the same within error (Figure 3C; Table S1), indicating that the M2-WT and M2−5Ala immobile conformations share similar membrane topology.

To further probe the membrane topology of the AH domains, we performed power saturation (PS) EPR experiments. The PS method measures changes in the relaxation efficiency of a spin label in the presence of paramagnetic reagents.[45] Because oxygen partitions into the hydrophobic environment of the bilayer, the collision rate of the spin label with O_2, quantified by the $\Delta P_{1/2}(O_2)$ parameter, serves as a measurement of membrane accessibility complementary to SR.[45] A comparison of the PS profiles of M2-WT and M2-5Ala sites is shown in Figure S2. Consistent with SR EPR results showing that the most populated conformation of M2-5Ala is shallower in the membrane than M2-WT, the M2-5Ala sites exhibit a lower oxygen accessibility than the corresponding M2-WT residues.

M2-5Ala Exhibits Altered Quaternary Arrangement within the Homotetramer.

The data presented above demonstrate that the AHs of M2-WT and M2-5Ala differ both in dynamics and membrane depth. We next explored whether M2-WT and M2-5Ala differ in the arrangement of AHs within the homotetramer.

DEER EPR can measure distances from ~20−60 Å and has been successfully applied to membrane proteins,[34,53] although resolving distances in homo-oligomeric proteins like M2 has proven to be challenging.[54] A single labeled site in a homotetramer with a single conformation would lead to two measurable distances resulting from subunits that are adjacent and diagonal in the tetramer (Figure S3). With the two distinct conformations of M2-WT identified by SR EPR measurements, we can thus predict four unique distances. However, because of the similar values of distances between symmetry-related sites within the homotetramer as predicted from published M2 structures[18] (Figure S4), a broad overlapped distribution may be expected.[54]

We collected DEER data for M2-WT and M2-5Ala AH sites 57 and 59. As shown in Figure 4 (black lines), the distance distributions of site 59 in M2-WT and M2-5Ala exhibit striking differences. The maximum of the distance distribution shifts from ~47 Å in M2-WT to ~27 Å in M2-5Ala, indicating a large rearrangement of subunits and/or rotation of the AHs within the homotetramer. The lack of well-defined oscillations within the time domain data, typical for membrane proteins in lipid bilayers, prevents the extraction of the four well-defined distances expected for two conformations of a homotetramer.[46,55] However, site 57 similarly exhibits a shift in DEER distance distributions (from a maximum of ~48 Å in M2-WT to ~34 Å in M2-5Ala; Figure S5), further supporting the existence of a large difference between M2-WT and M2-5Ala in the orientation of their C-terminal domains.

It is instructive to compare our experimental DEER data to a published SSNMR model M2-WT in lipid bilayers (PDB 2L0J).[18] We used mtsslWizard[56] to generate conformational ensembles of the site 57 and 59 spin labels in silico and simulate a distance distribution between the four symmetry-related sites (Figure S4). Overlays of the simulated distance distributions with experimental DEER data reveal marked differences. The simulated distribution for site 59 yields a broad peak at ~20 Å, which is a much shorter distance than the experimentally observed bimodal peaks at ~32 and ~47 Å. One possible reason for the discrepancy between our measured DEER distances and those simulated from the published SSNMR model is that the SSNMR model used a truncated construct M2(22–62), whereas our DEER data are for full-length M2. However, we also observed discrepancies between the SSNMR model and DEER distances in our previously published study on M2-WT(23–60).[39]

Cholesterol Immobilizes M2-WT while M2-5Ala is Insensitive to Cholesterol.

The M2 protein is proposed to bind cholesterol,[13,40] but biochemical studies have shown that M2-5Ala does not coimmunoprecipitate with cholesterol in vivo.[13] We compared how M2-WT and M2-5Ala respond in terms of conformation and dynamics to the addition of cholesterol.

In Figure 5A, we show CW EPR spectra of M2-WT and M2-5Ala in 4:1 POPC/POPG bilayers with (red) and without (black) cholesterol. In M2-WT, the addition of cholesterol to the membrane increases the relative intensity of the immobile component for sites 43 and 57. The site 59 line shape in M2-WT shows only minor changes between samples with and without cholesterol. We also spin-labeled three additional M2-WT AH sites (51, 55, and 60) and observed the general pattern that the growth in the immobile population is greatest for C-terminal sites close to the TM domain and becomes attenuated at distal residues (Figure S6). In a previous study using truncated M2-WT(23−−60), we also observed a shift toward a more immobile population of the AH in the presence of cholesterol.[39]

M2-5Ala line shapes both with and without cholesterol are shown in Figure 5B. Intriguingly, the 5Ala site 43 line shape is nearly superimposable in the presence and absence of cholesterol. For sites 57 and 59, the intensity of the immobile peak increases only slightly upon the addition of cholesterol, and the mobile population is still predominant.

We performed SR EPR experiments to assess whether the multicomponent nature of the CW line shapes in Figure 5 arises from conformational equilibria. The saturation curves for both M2-WT and M2-5Ala AHs in membranes with cholesterol are best characterized by biexponential fits with two unique spin−lattice relaxation rates (Figure S7), consistent with the existence of conformational exchange.

M2-5Ala Membrane Topology, Quaternary Arrangement, and CD Profiles are Insensitive to Cholesterol.

Unlike M2-WT, CW line shapes of M2-5Ala demonstrated no striking changes upon the addition of cholesterol. We next compared M2-WT and M2-5Ala responses to cholesterol in terms of membrane topology, quaternary arrangement, and CD profiles.

In a previous study using truncated M2-WT(23−60), we demonstrated that the AH shifts toward a conformation that is less membrane-buried in the presence of cholesterol.[39] Here we tested whether this observation was true for full-length M2-WT. As seen for truncated M2, all three of our full-length M2-WT sites (43, 57, and 59) exhibit decreased accessibility to oxygen in the presence of cholesterol (Figure S8). In marked contrast, the oxygen accessibilities of the same sites in M2-5Ala do not greatly change upon the addition of cholesterol (Figure S8), consistent with the highly attenuated ability of M2-5Ala to sense and respond to the presence of cholesterol.

Previously we demonstrated that the AHs in truncated M2-WT(23−60) become more tightly packed within the homotetramer in the presence of cholesterol.[39] The DEER data we collected here demonstrate that full-length M2-WT also becomes more tightly packed in the presence of cholesterol. Figures 4A (site 57) and S5 (site 59) show the distance distributions of M2-WT AH sites in membranes with (red lines) and without (black lines) cholesterol. Adding cholesterol to the membrane results in a shift toward shorter distances for M2-WT, consistent with the population shifting toward the more tightly packed conformation. In contrast, the addition of cholesterol causes only minor changes in the DEER distribution for M2-5Ala (Figures 4B and S5), which provides further evidence of the inability of M2-5Ala to sense and respond to the presence of cholesterol.

The CD profiles of M2-WT and M2-5Ala with and without cholesterol are shown in Figure S9. The CD spectra of both M2-WT and M2-5Ala without cholesterol exhibit two minima centered at 207 and 222 nm, which are characteristic of α-helical secondary structure.[52] Differences in the molar absorption between the M2-WT and M2-5Ala are subtle throughout the range investigated, suggesting that the five alanine mutations do not grossly alter the global secondary structure of the protein. Furthermore, changes in the molar absorption upon the addition of cholesterol to both M2-WT and M2-5Ala are minor, suggesting that global secondary structure does not change in the presence of cholesterol. CD spectral deconvolution shows no marked changes in helical character for either M2-WT and M2-5Ala upon the addition of cholesterol (Table S2).

DISCUSSION

M2-5Ala is deficient in viral budding. The inability of M2-5Ala to facilitate viral budding has been hypothesized to arise from the loss of AH−membrane interaction, altered sensitivity to cholesterol, and impaired “cross-talk” between different protein domains.[12–15,25] To our knowledge, we have for the first time experimentally tested each of these hypotheses through a detailed atomic-level comparison of the conformation, dynamics, and membrane topology of the full-length M2-WT and M2-5Ala proteins. We discuss each of these hypotheses in turn below. Finally, we describe a model for M2-facilitated viral budding wherein the membrane interaction of the AHs helps stabilize an arrangement of the TM helices necessary for proper budding.

Reduced Interaction of M2-5Ala with the Membrane Surface.

A common hypothesis for the loss of function observed with M2-5Ala is decreased interaction of the AH with the membrane surface. Replacing five hydrophobic residues of the AH with alanine reduces the hydrophobic moment of the helix (Figure 1B,C). A recent study demonstrated that a 16-residue M2-5Ala AH peptide did not insert as deeply into the membrane as the corresponding M2-WT sequence.[25] Results presented here for the full-length protein similarly show that the most highly populated conformation of M2-5Ala is not as closely associated with the membrane surface as M2-WT.

Interaction of AHs with membrane surfaces is critical in regulating curvature-sensing and curvature-inducing activity in a range of systems.[22,23,25,57] Mutations that disturb the hydrophobic properties of AHs have been shown to abolish membrane-remodeling activity.[12,15,25,58–63] However, the curvature-generating behavior of amphipathic helices in transmembrane proteins has not been as extensively studied.

Loss of Sensitivity of M2-5Ala to the Presence of Cholesterol.

Previously, we showed that truncated M2-WT(23−60) undergoes cholesterol-dependent conformational exchange in lipid bilayers.[39] M2-WT protein is proposed to bind cholesterol,[13,40] but biochemical studies have shown that M2-5Ala does not coimmunoprecipitate with cholesterol in vivo.[13] In this study, we sought to provide atomic-level conformational details to explain how M2-5Ala differs from M2-WT in its response to cholesterol.

We demonstrated that the addition of cholesterol to full-length M2-WT shifts the equilibrium toward the immobile component and changes the quaternary arrangement of the C-terminal domain. In contrast, M2-5Ala exhibits only minor changes in dynamics and quaternary arrangement when exposed to cholesterol.

The impact of cholesterol on M2-WT has been proposed to arise from changes in the membrane surrounding the protein and/or direct binding of cholesterol to the protein.[29,39,40,64] Cholesterol can have a range of impacts on lipid bilayer properties.[65] For example, a number of studies have shown that cholesterol has a condensing effect on membranes, which decreases the ability of membrane-associating helices to penetrate into the lipid headgroup region.[66–68] In M2-5Ala, the amphipathic helix is further away from the membrane surface and therefore is not as sensitive to changes in bilayer properties. Furthermore, there is some evidence for a specific cholesterol-binding site within the amphipathic helix in the M2 protein.[13,40] The alanine mutations could perturb the binding site and abolish the direct interaction of the protein with cholesterol.

Impaired Cross-Talk between Different Domains of M2-5Ala.

The AH domain of M2 alone can induce membrane curvature[15] and cause budding in giant unilamellar vesicles.[12] Full-length M2-WT, however, has an enhanced ability to generate curvature,[15] consistent with the TM domain enhancing curvature generation through protein shape effects.[15] Our structural work on the full-length M2 protein, both WT and a budding-deficient mutant, provides a unique opportunity to test the hypothesis that the domains of M2 work synergistically to induce curvature.

A cartoon schematic shown in Figure 6 summarizes a model that is consistent with our data. Shown on the left in Figure 6 are the most populated conformations of M2-WT and M2-5Ala in membranes without cholesterol. The M2-5Ala AHs (orange) are further from the membrane surface than the M2-WT AHs (red). Furthermore, M2-5Ala is more tightly packed than M2-WT. Although the mutations in M2-5Ala are in the C-terminal domain, the differences in the TM domain could arise from the AHs anchoring the TM helices into the membrane surface, effectively stabilizing one of several possible conformational states sampled by the TM helical bundle. A number of studies have shown that M2 TM domain can sample multiple structural substates.[29,36,69]

Shown on the right in Figure 6 are the most populated conformations of M2-WT and M2-5Ala in the presence of cholesterol. Our model for full-length M2-WT in cholesterol-containing membranes (Figure 6, top right) favors a conformation that is more compact than M2-WT in noncholesterol membranes, consistent with our previously published model of a budding-relevant M2 conformation based on SDSL-EPR data of M2(23−60).[39]

Our model for the conformation for M2-5Ala in cholesterol-containing membranes (Figure 6, bottom right) is very similar to the conformation of M2-5Ala in membranes without cholesterol (Figure 6, bottom left). The lack of membrane interaction of the AHs of M2-5Ala eliminates interdomain coupling needed for the TM domain to respond to the presence of cholesterol.

We have traced in blue the membrane interaction domains of our models for M2-WT and M2–5A in the presence of cholesterol. M2-WT forms a conical, or wedge-like shape (see also Figure S4). In contrast to M2-WT, we propose M2-5Ala forms a cylindrical shape resulting from the lack of membrane interaction of the AHs. The ability to form a wedge shape was previously hypothesized to play a role in M2's ability to generate curvature.[15] When a transmembrane protein forms a wedge within a lipid bilayer, it can exclude different volumes in the two bilayer leaflets and dynamically induce membrane curvature.[24]

SUMMARY

We have provided new insight into the mechanism of M2-facilitated budding using a multipronged SDSL-EPR approach. Numerous studies have characterized the functional deficiencies of M2-5Ala[12–15,25] but the unique contribution of this study is the detailed atomic-level comparison of the conformation, dynamics, and membrane topology of M2-WT and the budding-deficient M2 mutant (M2-5Ala). Our use of full-length protein in membranes has allowed us to test the hypothesis that the AH and TM domains of M2 work synergistically to induce membrane curvature. A model consistent with our data incorporates coupling between the AH and TM domains of M2. We propose interdomain coupling is necessary for the protein to respond to the presence of cholesterol and generate an overall protein shape that facilitates viral budding.[15] M2 plays a key role in the replication cycle of the influenza virus. Antagonizing the dynamic properties of the AH that enable interdomain coupling may therefore represent a novel strategy for anti-influenza drug design.

Supplementary Material

Refer to Web version on PubMed Central for supplementary material.

ACKNOWLEDGMENTS

We gratefully acknowledge Sangwoo S. Kim, Phuong A. Nguyen and Nathan W. Schmidt for critical reading of the manuscript and helpful comments.

Funding

This work was generously supported by the National Institutes of Health Grants AI117657–01 (to K.P.H.), R01 GM108026 (to G.A.L) and P41 EB001980 (J.B.F and the National Biomedical EPR Center). Funding was also provided by the National Science Foundation Grant CHE-1305664 (to G.A.L). G.A.L. would like to acknowledge support from the John W. Steube Professorship.

ABBREVIATIONS

SDSL-EPR	site-directed spin labeling electron paramagnetic resonance spectroscopy
SSNMR	solid-state NMR
TM	transmembrane
AH	amphipathic helix
WT	wild-type
POPC	1-palmitoyl-2-oleoyl-sn-glycero-3-phosphocholine
POPG	1-palmitoyl-2-oleoyl-sn-glycero-3-phospho-1-rac-glycerol
CW EPR	continuous-wave electron paramagnetic reso nance
SR EPR	saturation recovery electron paramagnetic resonance
DEER	double electron−electron resonance
CD	circular dichroism
PS	power saturation
DHPC	1,2-dihexanoyl-sn-glycero-3-phosphocholine

REFERENCES

(1). Alvarado De La Barrera C, and Reyes-Teran G (2005) Influenza: Forecast for a pandemic. Arch. Med. Res 36, 628–636. [PubMed: 16216644]

(2). Fukuyama S, and Kawaoka Y (2011) The pathogenesis of influenza virus infections: The contributions of virus and host factors. Curr. Opin. Immunol 23, 481–486. [PubMed: 21840185]

(3). Rossman JS, and Lamb RA (2011) Influenza virus assembly and budding. Virology 411, 229–236. [PubMed: 21237476]

(4). Pinto LH, and Lamb RA (2006) The M2 proton channels of influenza A and B viruses. J. Biol. Chem 281, 8997–9000. [PubMed: 16407184]

(5). Wang D, Harmon A, Jin J, Francis DH, Christopher-Hennings J, Nelson E, Montelaro RC, and Li F (2010) The lack of an inherent membrane targeting signal is responsible for the failure of the matrix (M1) protein of influenza A virus to bud into virus-like particles. J. Virol 84, 4673–81. [PubMed: 20181696]

(6). Leser GP, and Lamb RA (2017) The lateral organization of influenza virus proteins in the budozone region of the plasma membrane. J. Virol 91, e02104–16. [PubMed: 28202765]

(7). Grantham ML, Stewart SM, Lalime EN, and Pekosz A (2010) Tyrosines in the Influenza A Virus M2 protein cytoplasmic tail are critical for production of infectious virus particles. J. Virol 84, 8765–8776. [PubMed: 20573832]

(8). Chen BJ, Leser GP, Jackson D, and Lamb RA (2008) The Influenza virus M2 protein cytoplasmic tail interacts with the M1 protein and influences virus assembly at the site of virus budding. J. Virol 82, 10059–10070. [PubMed: 18701586]

(9). McCown MF, and Pekosz A (2006) Distinct domains of the influenza A virus M2 protein cytoplasmic tail mediate binding to the M1 protein and facilitate infectious virus production. J. Virol 80, 8178–8189. [PubMed: 16873274]

(10). Iwatsuki-Horimoto K, Horimoto T, Noda T, Kiso M, Maeda J, Watanabe S, Muramoto Y, Fujii K, and Kawaoka Y (2006) The cytoplasmic tail of the influenza A virus M2 protein plays a role in viral assembly. J. Virol 80, 5233–5240. [PubMed: 16699003]

(11). Gautier R, Douguet D, Antonny B, and Drin G (2008) HELIQUEST: a web server to screen sequences with specific α-helical properties. Bioinformatics 24, 2101–2102. [PubMed: 18662927]

(12). Rossman JS, Jing XH, Leser GP, and Lamb RA (2010) Influenza virus M2 protein mediates ESCRT-independent membrane scission. Cell 142, 902–913. [PubMed: 20850012]

(13). Rossman JS, Jing XH, Leser GP, Balannik V, Pinto LH, and Lamb RA (2010) Influenza virus M2 ion channel protein is necessary for filamentous virion formation. J. Virol 84, 5078–5088. [PubMed: 20219914]

(14). Roberts KL, Leser GP, Ma C, and Lamb RA (2013) The amphipathic helix of influenza A virus M2 protein is required for filamentous bud formation and scission of filamentous and spherical particles. J. Virol 87, 9973–82. [PubMed: 23843641]

(15). Schmidt NW, Mishra A, Wang J, DeGrado WF, and Wong GCL (2013) Influenza virus A M2 protein generates Negative Gaussian membrane curvature necessary for budding and scission. J. Am. Chem. Soc 135, 13710–13719. [PubMed: 23962302]

(16). Schnell JR, and Chou JJ (2008) Structure and mechanism of the M2 proton channel of influenza A virus. Nature 451, 591–595. [PubMed: 18235503]

(17). Claridge JK, Aittoniemi J, Cooper DM, and Schnell JR (2013) Isotropic bicelles stabilize the juxtamembrane region of the influenza M2 protein for solution NMR studies. Biochemistry 52, 8420–8429. [PubMed: 24168642]

(18). Sharma M, Yi M, Dong H, Qin H, Peterson E, Busath DD, Zhou H-X, and Cross TA (2010) Insight into the mechanism of the influenza A proton channel from a structure in a lipid bilayer. Science 330, 509–512. [PubMed: 20966252]

(19). Tian C, Gao PF, Pinto LH, Lamb RA, and Cross TA (2003) Initial structural and dynamic characterization of the M2 protein transmembrane and amphipathic helices in lipid bilayers. Protein Sci 12, 2597–2605. [PubMed: 14573870]

(20). Nguyen PA, Soto CS, Polishchuk A, Caputo GA, Tatko CD, Ma CL, Ohigashi Y, Pinto LH, DeGrado WF, and Howard KP (2008) pH-induced conformational change of the influenza M2 protein C-terminal domain. Biochemistry 47, 9934–9936. [PubMed: 18754675]

(21). Huang S, Green B, Thompson M, Chen R, Thomaston J, DeGrado WF, and Howard KP (2015) C-terminal juxtamembrane region of full-length M2 protein forms a membrane surface associated amphipathic helix. Protein Sci 24, 426–429. [PubMed: 25545360]

(22). Drin G, Casella J-F, Gautier R, Boehmer T, Schwartz TU, and Antonny B (2007) A general amphipathic α-helical motif for sensing membrane curvature. Nat. Struct. Mol. Biol 14, 138–146. [PubMed: 17220896]

(23). Drin G, and Antonny B (2010) Amphipathic helices and membrane curvature. FEBS Lett 584, 1840–1847. [PubMed: 19837069]

(24). McMahon HT, and Gallop JL (2005) Membrane curvature and mechanisms of dynamic cell membrane remodelling. Nature 438, 590–596. [PubMed: 16319878]

(25). Martyna A, Bahsoun B, Badham MD, Srinivasan S, Howard MJ, and Rossman JS (2017) Membrane remodeling by the M2 amphipathic helix drives influenza virus membrane scission. Sci. Rep 7, 44695. [PubMed: 28317901]

(26). Ma C, Polishchuk AL, Ohigashi Y, Stouffer AL, Schön A, Magavern E, Jing X, Lear JD, Freire E, Lamb RA, DeGrado WF, and Pinto LH (2009) Identification of the functional core of the influenza A virus A/M2 proton-selective ion channel. Proc. Natl. Acad. Sci. U. S. A 106, 12283–8. [PubMed: 19590009]

(27). Stouffer AL, Acharya R, Salom D, Levine AS, Di Costanzo L, Soto CS, Tereshko V, Nanda V, Stayrook S, and DeGrado WF (2008) Structural basis for the function and inhibition of an influenza virus proton channel. Nature 451, 596–9. [PubMed: 18235504]

(28). Acharya R, Carnevale V, Fiorin G, Levine BG, Polishchuk AL, Balannik V, Samish I, Lamb RA, Pinto LH, DeGrado WF, and Klein ML (2010) Structure and mechanism of proton transport through the transmembrane tetrameric M2 protein bundle of the influenza A virus. Proc. Natl. Acad. Sci. U. S. A 107, 15075–80. [PubMed: 20689043]

(29). Hu F, Luo W, Cady SD, and Hong M (2011) Conformational plasticity of the influenza A M2 transmembrane helix in lipid bilayers under varying pH, drug binding, and membrane thickness. Biochim. Biophys. Acta, Biomembr 1808, 415–423.

(30). Andreas LB, Eddy MT, Pielak RM, Chou J, and Griffin RG (2010) Magic angle spinning NMR investigation of Influenza A M2 18−60: support for an allosteric mechanism of inhibition. J. Am. Chem. Soc 132, 10958–10960. [PubMed: 20698642]

(31). Cady S, Wang T, and Hong M (2011) Membrane-dependent effects of a cytoplasmic helix on the structure and drug binding of the influenza virus M2 protein. J. Am. Chem. Soc 133, 11572–11579. [PubMed: 21661724]

(32). Kwon B, Tietze D, White PB, Liao SY, and Hong M (2015) Chemical ligation of the influenza M2 protein for solid-state NMR characterization of the cytoplasmic domain. Protein Sci 24, 1087–1099. [PubMed: 25966817]

(33). Bordignon E (2011) Site-Directed spin labeling of membrane proteins. Top. Curr. Chem 321, 121–157.

(34). Claxton DP, Kazmier K, Mishra S, and McHaourab HS (2015) Navigating membrane protein structure, dynamics, and energy landscapes using spin labeling and EPR spectroscopy. Methods Enzymol 564, 349–387. [PubMed: 26477257]

(35). Bridges MD, Hideg K, and Hubbell WL (2010) Resolving conformational and rotameric exchange in spin-labeled proteins using saturation recovery EPR. Appl. Magn. Reson 37, 363–390. [PubMed: 20157634]

(36). Duong-Ly KC, Nanda V, Degrado WF, and Howard KP (2005) The conformation of the pore region of the M2 proton channel depends on lipid bilayer environment. Protein Sci 14, 856–861. [PubMed: 15741338]

(37). Thomaston JL, Nguyen PA, Brown EC, Upshur MA, Wang J, DeGrado WF, and Howard KP (2013) Detection of drug-induced conformational change of a transmembrane protein in lipid bilayers using site-directed spin labeling. Protein Sci 22, 65–73. [PubMed: 23139077]

(38). Saotome K, Duong-Ly KC, and Howard KP (2015) Influenza A M2 protein conformation depends on choice of model membrane. Biopolymers 104, 405–411. [PubMed: 25652904]

(39). Kim SS, Upshur MA, Saotome K, Sahu ID, McCarrick RM, Feix JB, Lorigan GA, and Howard KP (2015) Cholesterol-dependent conformational exchange of the C-terminal domain of the Influenza A M2 protein. Biochemistry 54, 7157–7167. [PubMed: 26569023]

(40). Schroeder C, Heider H, Moncke-Buchner E, and Lin TI (2005) The influenza virus ion channel and maturation cofactor M2 is a cholesterol-binding protein. Eur. Biophys. J 34, 52–66. [PubMed: 15221235]

(41). Gerl MJ, Sampaio JL, Urban S, Kalvodova L, Verbavatz J-M, Binnington B, Lindemann D, Lingwood CA, Shevchenko A, Schroeder C, and Simons K (2012) Quantitative analysis of the lipidomes of the influenza virus envelope and MDCK cell apical membrane. J. Cell Biol 196, 213–21. [PubMed: 22249292]

(42). Leiding T, Wang J, Martinsson J, DeGrado WF, and Arsköld SP (2010) Proton and cation transport activity of the M2 proton channel from influenza A virus. Proc. Natl. Acad. Sci. U. S. A 107, 15409–14. [PubMed: 20713739]

(43). Pinto LH, Dieckmann GR, Gandhi CS, Papworth CG, Braman J, Shaughnessy MA, Lear JD, Lamb RA, and DeGrado WF (1997) A functionally defined model for the M2 proton channel of influenza A virus suggests a mechanism for its ion selectivity. Proc. Natl. Acad. Sci. U. S. A 94, 11301–11306. [PubMed: 9326604]

(44). Shuck K, Lamb RA, and Pinto LH (2000) Analysis of the pore structure of the influenza A virus M(2) ion channel by the substituted-cysteine accessibility method. J. Virol 74, 7755–7761. [PubMed: 10933681]

(45). Klug CS, and Feix JB (2008) Methods and applications of site-directed spin labeling EPR spectroscopy, in Biophysical Tools for Biologists: Vol. 1 In Vitro Techniques, pp 617–658, Elsevier Academic Press Inc, San Diego, CA.

(46). Sahu ID, McCarrick RM, Troxel KR, Zhang R, Smith HJ, Dunagan MM, Swartz MS, Rajan PV, Kroncke BM, Sanders CR, and Lorigan GA (2013) DEER EPR measurements for membrane protein structures via bifunctional spin labels and lipodisq nanoparticles. Biochemistry 52, 6627–6632. [PubMed: 23984855]

(47). Jeschke G, Chechik V, Ionita P, Godt A, Zimmermann H, Banham J, Timmel CR, Hilger D, and Jung H (2006) DeerAnalysis2006 - a comprehensive software package for analyzing pulsed ELDOR data. Appl. Magn. Reson 30, 473–498.

(48). Chiang YW, Borbat PP, and Freed JH (2005) The determination of pair distance distributions by pulsed ESR using Tikhonov regularization. J. Magn. Reson 172, 279–295. [PubMed: 15649755]

(49). Whitmore L, and Wallace BA (2004) DICHROWEB, an online server for protein secondary structure analyses from circular dichroism spectroscopic data. Nucleic Acids Res 32, W668–73. [PubMed: 15215473]

(50). Sreerama N, and Woody RW (2000) Estimation of protein secondary structure from circular dichroism spectra: comparison of CONTIN, SELCON, and CDSSTR methods with an expanded reference set. Anal. Biochem 287, 252–260. [PubMed: 11112271]

(51). Abdul-Gader A, Miles AJ, and Wallace BA (2011) A reference dataset for the analyses of membrane protein secondary structures and transmembrane residuesusing circular dichroism spectroscopy. Bioinformatics 27, 1630–1636. [PubMed: 21505036]

(52). Miles AJ, and Wallace BA (2016) Circular dichroism spectroscopy of membrane proteins. Chem. Soc. Rev 45, 4859–4872. [PubMed: 27347568]

(53). McHaourab HS, Steed PR, and Kazmier K (2011) Toward the fourth dimension of membrane protein structure: Insight into dynamics from spin-labeling EPR spectroscopy. Structure 19, 1549–1561. [PubMed: 22078555]

(54). Dalmas O, Hyde HC, Hulse RE, and Perozo E (2012) Symmetry-constrained analysis of pulsed double electron−electron resonance (DEER) spectroscopy reveals the dynamic nature of the KcsA activation gate. J. Am. Chem. Soc 134, 16360–16369. [PubMed: 22946877]

(55). Jeschke G (2012) DEER Distance Measurements on Proteins. Annu. Rev. Phys. Chem 63, 419–446. [PubMed: 22404592]

(56). Hagelueken G, Ward R, Naismith JH, and Schiemann O (2012) MtsslWizard: in silico spin-labeling and generation of distance distributions in PyMOL. Appl. Magn. Reson 42, 377–391. [PubMed: 22448103]

(57). Zimmerberg J, and Kozlov MM (2006) How proteins produce cellular membrane curvature. Nat. Rev. Mol. Cell Biol 7, 9–19. [PubMed: 16365634]

(58). Farsad K, Ringstad N, Takei K, Floyd SR, Rose K, and De Camilli P (2001) Generation of high curvature membranes mediated by direct endophilin bilayer interactions. J. Cell Biol 155, 193–200. [PubMed: 11604418]

(59). Peter BJ, Kent HM, Mills IG, Vallis Y, Butler PJG, Evans PR, and McMahon HT (2004) BAR domains as sensors of membrane curvature: the amphiphysin BAR structure. Science 303, 495–499. [PubMed: 14645856]

(60). Lee MCS, Orci L, Hamamoto S, Futai E, Ravazzola M, and Schekman R (2005) Sar1p N-terminal helix initiates membrane curvature and completes the fission of a COPII vesicle. Cell 122, 605–617. [PubMed: 16122427]

(61). Fernandez-Vidal M, Jayasinghe S, Ladokhin AS, and White SH (2007) Folding amphipathic helices into membranes: amphiphilicity trumps hydrophobicity. J. Mol. Biol 370, 459–70. [PubMed: 17532340]

(62). Chong SSY, Taneva SG, Lee JMC, and Cornell RB (2014) The curvature sensitivity of a membrane-binding amphipathic helix can be modulated by the charge on a flanking region. Biochemistry 53, 450–461. [PubMed: 24397368]

(63). Vanni S, Vamparys L, Gautier R, Drin G, Etchebest C, Fuchs PFJ, and Antonny B (2013) Amphipathic lipid packing sensor motifs: probing bilayer defects with hydrophobic residues. Biophys. J 104, 575–584. [PubMed: 23442908]

(64). Ekanayake EV, Fu R, and Cross TA (2016) Structural influences: cholesterol, drug, and proton binding to full-length Influenza A M2 protein. Biophys. J 110, 1391–1399. [PubMed: 27028648]

(65). Krause MR, and Regen SL (2014) The structural role of cholesterol in cell membranes: From condensed bilayers to lipid rafts. Acc. Chem. Res 47, 3512–3521. [PubMed: 25310179]

(66). Dennison SR, and Phoenix DA (2011) Effect of cholesterol on the membrane interaction of modelin-5 isoforms. Biochemistry 50, 10898–10909. [PubMed: 22082130]

(67). Sood R, and Kinnunen PKJ (2008) Cholesterol, lanosterol, and ergosterol attenuate the membrane association of LL-37(W27F) and temporin L. Biochim. Biophys. Acta, Biomembr 1778, 1460–1466.

(68). Monette M, Van Calsteren MR, and Lafleur M (1993) Effect of cholesterol on the polymorphism of dipalmitoylphosphatidylcholine/melittin complexes: an NMR study. Biochim. Biophys. Acta, Biomembr 1149, 319–328.

(69). Yi M, Cross TA, and Zhou H-X (2009) Conformational heterogeneity of the M2 proton channel and a structural model for channel activation. Proc. Natl. Acad. Sci. U. S. A 106, 13311–13316. [PubMed: 19633188]

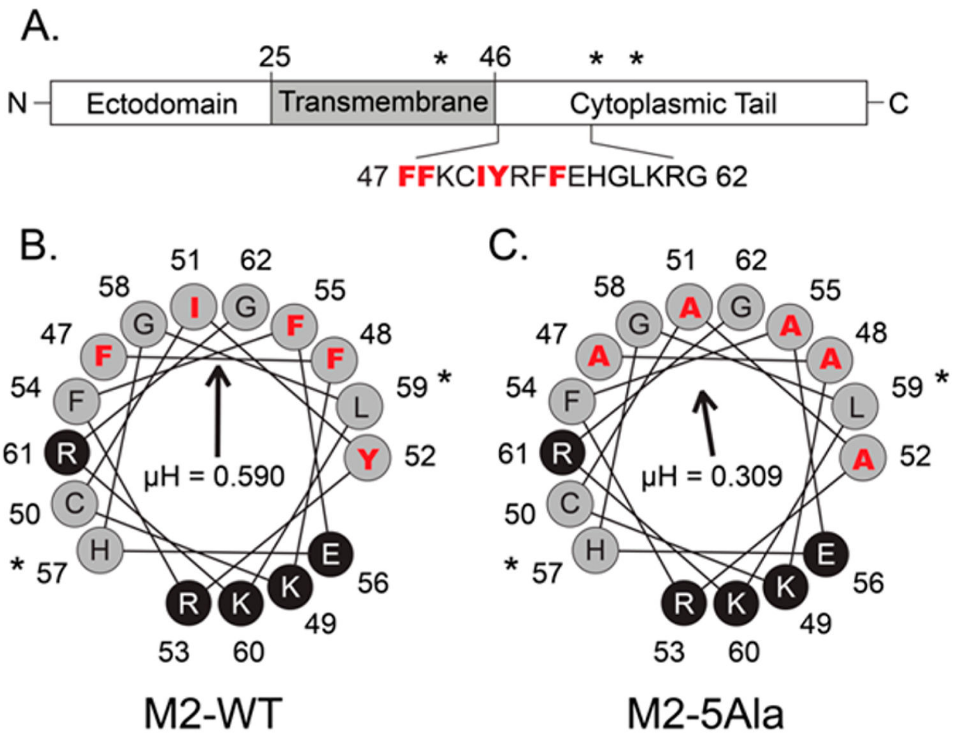

Figure 1.

Domain structure of the M2 protein monomer studied here. In vivo, M2 functions as a homotetramer. (A) Each M2 monomer consists of an N-terminal ectodomain, a transmembrane domain, and a C-terminal cytoplasmic domain. The sequence of the 16 residues comprising the amphipathic helix (sites 47−62) is shown. Residues in red are mutated to alanine in M2-5Ala (F47A, F48A, I51A, Y52A, and F55A). Asterisks (*) represent sites (L43, H57, L59) selected for spin labeling studies. (B) Helical wheel diagrams and hydrophobic moments (μH) of the M2-WT and (C) M2-5Ala amphipathic helices created by HeliQuest.[11] Residues charged at pH 7.8 are shown in black, and uncharged residues are shown in gray.

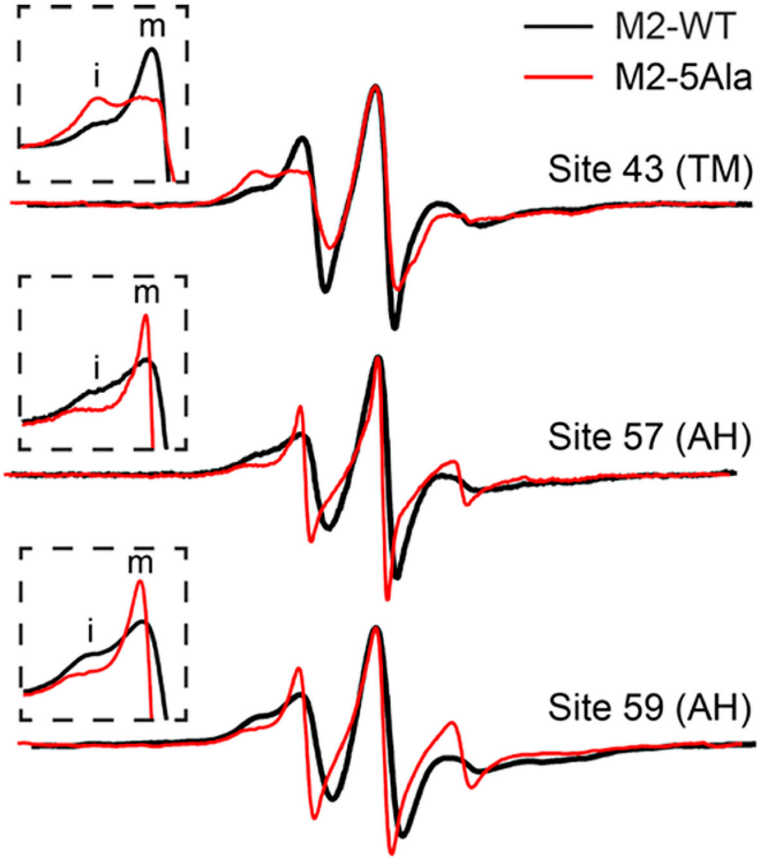

Figure 2.

EPR line shapes indicate TM site 43 is immobilized in M2-5Ala relative to M2-WT, while AH sites 57 and 59 are more mobile in M2-5Ala relative to M2-WT. X-band CW EPR spectra of M2-WT and M2-5Ala in 4:1 POPC/POPG bilayers. Each sample contains, on average, one spin-labeled monomer per tetramer. Inset shows the low-field immobile (i) and mobile (m) peak components.

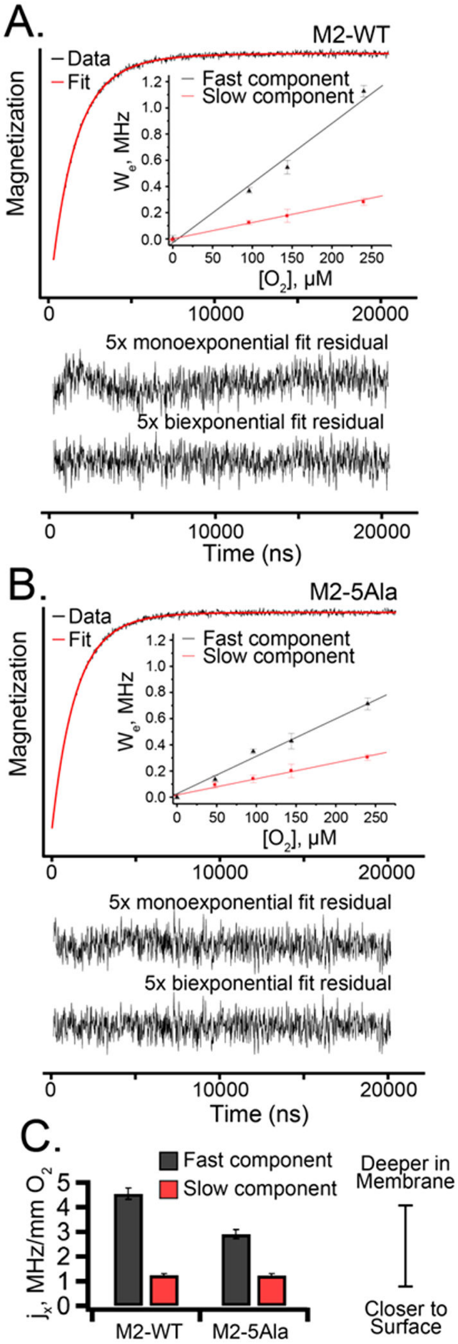

Figure 3.

M2-WT and M2-5Ala exhibit two components in conformational exchange. (A) Representative saturation-recovery data and fit for site 59 of M2-WT and (B) M2-5Ala in 4:1 POPC/POPG bilayers under 40% air. Residuals for mono- and biexponential fits are shown below the curve. Inset shows the dependence of W_e on the concentration of O_2 for the fast, mobile component (black) and slow, immobile component (red). (C) Oxygen accessibility determined from the slopes of the linear best fit lines of data shown in the insets.

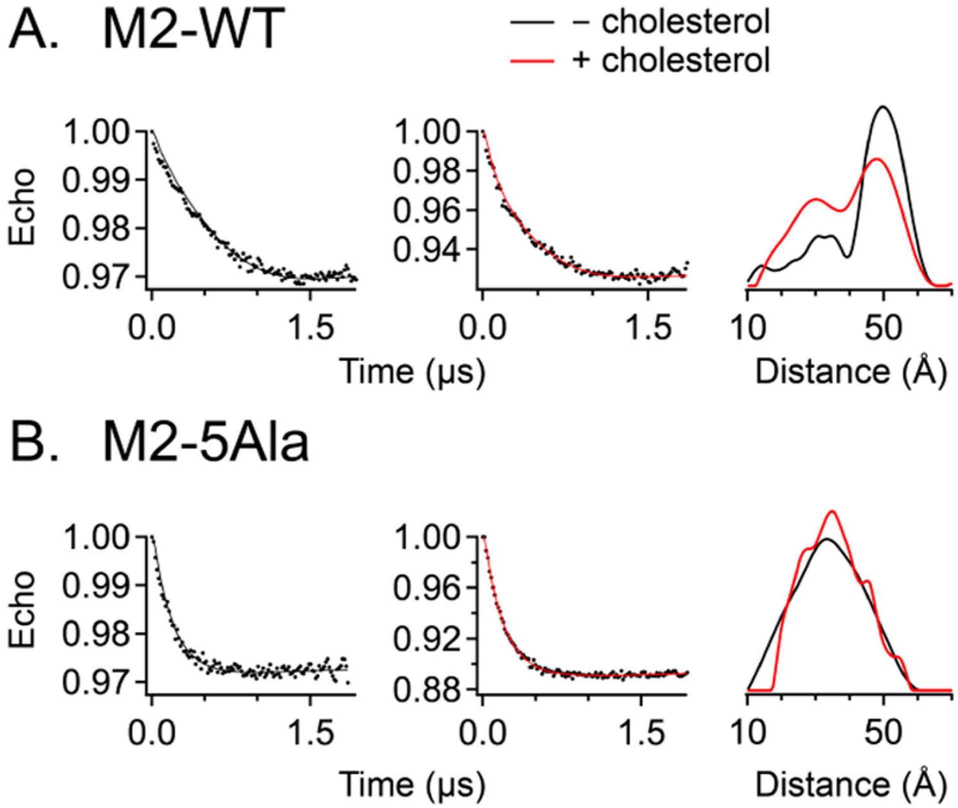

Figure 4.

DEER reveals different distance distributions of spin-labeled site 59 of (A) M2-WT and (B) M2-5Ala reconstituted into 4:1 POPC/POPG bilayers without (−) or with (+) cholesterol. Background-subtracted dipolar evolution data are shown as black dots with the corresponding fits as solid lines. Overlaid distance distributions were normalized to the area under the curve. Distances below 20 Å fall below the reliable detection limit of DEER.

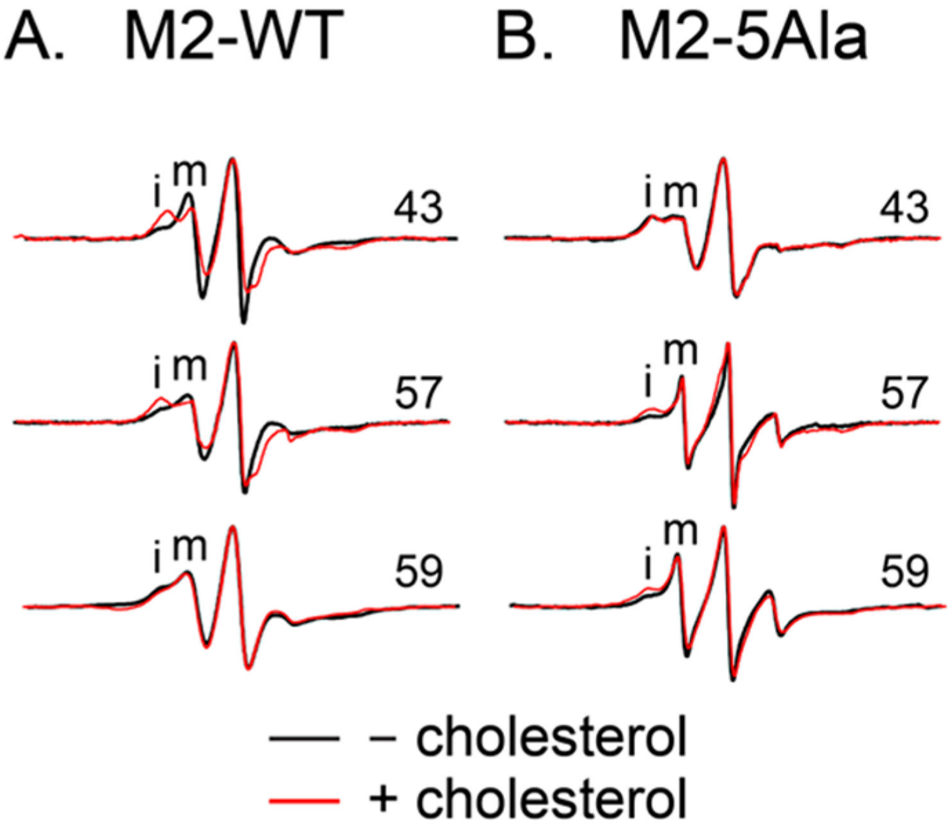

Figure 5.

M2-WT and M2-5Ala CW line shapes exhibit differing sensitivity to cholesterol. CW EPR spectra of (A) M2-WT and (B) M2-5Ala in bilayers without (−) or with (+) cholesterol. The low-field immobile (i) and mobile (m) component peaks are indicated.

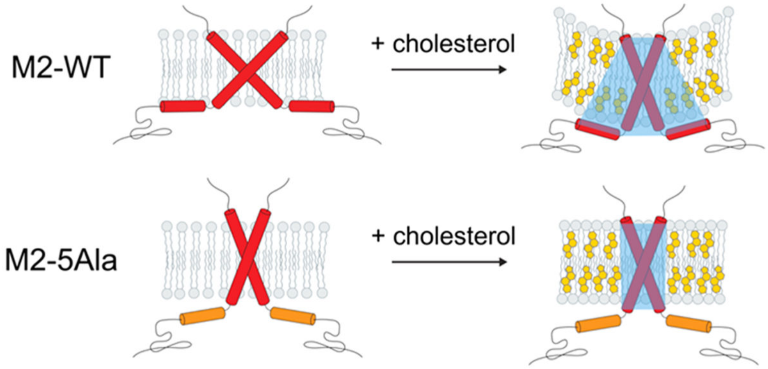

Figure 6.

A cartoon model consistent with experimental data collected from the M2-WT and M2-5Ala AH and TM domains. For clarity only two of the four subunits of the M2 homotetramer are shown. Furthermore, only the most populated conformation for each set of conditions is shown. The addition of cholesterol to the membrane shifts the M2-WT AH population toward a more compact conformation. Coupling between the AH and TM causes M2-WT to adopt a wedge-like shape that promotes curvature, shaded in blue. The M2-5Ala AH do not interact closely with the membrane surface, and consequently the conformation of M2-5Ala is insensitive to bilayer properties.